Effects of irradiation with nickel Ions in the microstructure and superficial composition of DIN 1.4970 austenitic steel irradiated at high doses and temperatures

N. A. Flores-Fuentes[a], C. Juárez-León[a], Á. Morales-González[a], J. M. Tirado-Lule[a], J. A. Morales-González[b], R. Vázquez-Arreguín[a], E. O. Madrigal-Santillán[b], L. Anguiano-Robledo[c], L. Delgado Olivares[d], and E. O. López-de-León[e]

[a]*Escuela Superior de Cómputo, Instituto Politécnico Nacional, Av. Juan de Dios Bátiz s/n Esquina Miguel Othón de Mendizabal, Unidad Profesional Adolfo López Mateos, Ciudad de México 07738, México,*
[b]*Laboratorio de Medicina de Conservación, Escuela Superior de Medicina, Instituto Politécnico Nacional, México, Plan de San Luis y Díaz Mirón, Col. Casco de Santo Tomás, Del. Miguel Hidalgo, Ciudad de México 11340, México,*
[c]*Escuela Superior de Medicina, Laboratorio de Farmacología Molecular, Instituto Politécnico Nacional, Alcaldía Miguel Hidalgo, Ciudad de México 11340, México,*
[d]*Centro de Investigación Interdisciplinario, Área Académica de Nutrición, Instituto de Ciencias de la Salud, Universidad Autónoma del Estado de Hidalgo, Circuito Ex hacienda La Concepción S/N, Carretera Pachuca-Actopan, San Agustín Tlaxiaca, Hidalgo, 42160, México,*
[e]*Centro Interdisciplinario de Ciencias de la Salud - Unidad Milpa Alta, Instituto Politécnico Nacional, México.*

Received 02 February 2024; accepted 16 May 2025

In this work, we conducted a study on the microstructural and compositional changes on the surface of German Institute for Standardization in English (DIN) 1.4970 Austenitic Steel irradiated with Nickel (Ni) ions at a dose of 360 (dpa) and a temperature of 650°C. We employed techniques of S diffraction in Grazing X-Ray Diffraction (GXRD) and X-ray Photoelectron Spectros-copy (XPS) to characterize the surface of the steel after each treatment. The study found that the concentration of iron (Fe) and chromium (Cr) in the Non-Irradiated Zone (NIZ) was greater with respect to the Irradiated Zone (IZ), while the concentration of the elements Nickel (Ni) and Silicon (Si) in the NIZ is lesser with respect to the IZ. In addition, there was a decrease of Fe and Cr and an increase of Ni and Si due to the irradiation. The damage caused by the Ni ions to the DIN 1.4970 steel is found at 1.560 μm below the surface.

Keywords: Grazing Incidence X-Ray Diffraction; XPS; irradiation; austenitic stainless steel; materials; TEM; SEM.

DOI: https://doi.org/10.31349/RevMexFis.72.031002

1. Introduction

The constant bombing of neutrons in nuclear reactors gives rise to damages and transformations in the materials of the reactor's walls, which affects their mechanical properties and reduces durability. This poses a risk for the integrity of the reactor, which renders the selection of materials crucial. The austenitic stainless steels have been widely adopted in these ambits due to their outstanding resistance and tenacity, together with their durability along extended periods of operation [1–4].

These alloys present a series of advantages, including high resistance to creeping, microstructural stability [5], and resistance to void swelling [6, 7]. The addition of stabilizing elements to these steels exerts beneficial effects, such as the prevention of intergranular corrosion and the reduction of void swelling [1–8]. Notwithstanding this, austenitic steels are susceptible to cracking because of intergranular corrosion, especially under irradiation, because of the formation of chromium carbide precipitates in the grain boundaries, which diminishes the concentration of chromium in those areas [9–11].

Irradiation of Titanium (Ti)-stabilized austenitic steels have demonstrated the induction of segregation and precipitation. At high irradiation temperatures, we may observe the nucleation of Titanium Chloride (TiC) precipitates enriched with nanometric-size chromium (Cr), surrounded by silicon (Si)- and nickel (NI)- rich layers [5, 12–15]. The addition of titanium diminishes the mobility of the vacant layers and contributes to better resistance to swelling, because the Titanium Carbide (TiC) acts as a drain for the helium bubbles, which are the causes of the cracking in irradiated steels [12, 16].

However, one principal inconvenience of austenitic steels utilized as coating is their propensity toward volumetric swelling [17]. Nucleation of the TiC to the degree that they precipitate nanometric-size MultiChannels (MC) in the network defects, such as dislocations, is a phenomenon that should be taken into consideration [5, 18].

The transition of the incubation stage to the stationary stage is commonly associated with "microstructural instability", characterized by the formation of various phases induced by the radiation and later the exhaustion of certain elements of the alloy in the matrix [19]. Investigations have also been conducted on the behavior of the oxi-

dation of the different nuclear-grade steels, austenitic as well as ferritic/martensitic steels, after their exposure to oxidant surroundings, such as liquid Lead-Bismuth Ententic (LBE) [20–22].

It has been observed that Concentrated Solid solution Alloys (CSA) and High Entropy Alloys (HEA) offer unique properties, such as high resistance to radiation and to corrosion at high temperatures, in comparison with the conventional materials utilized in nuclear components [23, 24]. However, in terms of those currently available for light-water reactors, the austenitic stainless steels do not appear to satisfy the demands of prolonged operation at high temperatures in next-generation nuclear-energy systems [25].

Diverse studies have been focused on the alloys of face-centered cubic (fcc) solid-type solutions, specifically CoCrFeNiMnx (x = 0,7, 1, 1,3), as a possible alternative in the development of materials for nuclear reactors. Additionally, austenitic Stainless Steel 316 (316SS) is included as a point of reference, in that it has been investigated under numerous irradiation conditions [26–28].

Damage due to irradiation by ions in austenitic steels has been widely studied through Transmission Electronic Microscopy (TEM) techniques [29–31], as well as by superficial techniques, such as Grazing X-Ray Diffraction (GXRD) and XPS [11, 14, 32–36]. With these types of techniques, information may be obtained on the damage caused by the irradiation in function of the depth, which allows for analyzing the micro-structural and compositional changes of austenitic steels, such as German Institute of Standardization in English (DIN) 1.4970.

The austenitic stainless steels have been fundamental in nuclear reactors because of their resistance and tenacity. However, they face challenges in terms of corrosion, swelling, and resistance to irradiation. On-going investigations center on overcoming these limitations and developing novel materials that comply with the operational requisites of next-generation nuclear reactors.

Through the application of the X-ray Photoelectron Spectroscopy (XPS) technique, the expectation is to obtain depth-function concentration profiles, which will allow the observation of the variation of elements such as Iron (Fe), Chromium (Cr), Nickel (Ni), and Silicon (Si) in the analyzed austenitic stainless steel. Particularly, a diminution of Cr is foreseen, together with an increase of Ni and Si toward the surface of the Irradiated Zone (IZ). In addition, in the Grazing Incidence X Ray Diffraction (GIXRD) analysis, by modifying the angle of incidence of the X rays, will render possible the intensity of the diffraction peaks of DIN 1.4970 austenitic (au) stainless steel with respect to the depth. On the other hand, given that the sample of DIN 1.4970 steel was prepared in transversal section by means of the Focused Ion Beam (FIB) technique until reaching a thickness of 200 nm, a Transmission Electron Microscopy (TEM) analysis will be able to be conducted to identify directly the Non-Irradiated Zone (NIZ), permitting the observation of the defects generated by the irradiation with Ni ions and the direct measurement of the maximal damage depth in the austenitic steel. In this sense, this is expected to evidence a variation in defect density vis-à-vis the depth, achieving an approximate maximum of 1.2 μm, according to simulations carried out with SRIM software [http://www.srim.org/index.htm].

DIN 1.4970 austenitic stainless steel maintains the retained austenite at room temperature, which confers greater structural stability in extreme environments, such as nuclear reactors, in comparison with other austenitic stainless steels. Its high content of Chromium (Cr) contributes to its resistance to oxidation and to corrosion at high temperatures, forming a protective oxide layer. The irradiation gives rise to an increase of Cr with the depth, coinciding with the mechanisms of the migration of elements observed in other studies. Advanced techniques such as Transmission Electron Microscopy (TEM) allow for the identification of Irradiated Zones (IZ) and Non-Irradiated Zones (NIZ) and for measuring the maximal damage depth of approximately 1.2 μm, providing a detailed analysis at the microscopic level. In sum, DIN 1.4970 austenitic stainless steel is highlighted for its structural stability and its resistance to irradiation, comprising a preferable option for applications in nuclear reactors. Its behavior in the face of irradiation and the variation in the concentration of elements such as Cr and Nickel (Ni) offer a deeper understanding of its capacity to bear up under extreme conditions, complying with the requisites for resistance to corrosion and thermal stability.

2. Materials and methods

2.1. Materials

In this work, we employed a DIN 1.4970 austenitic steel (65.5Fe14.1Ni16.35Cr1.9Mn0.8Mo0.6Si0.35Ti0.4C, % at.) the density of which is 7.91 g/cm^3, and it possesses a face-centered cubic (fcc) crystalline structure with a network parameter of $a = 3.585$ Å [37]. The sample was thinned by cold rolling at 15%, and to avoid fragilization, we alternated annealings that recover the ductility of the material. This was repeated until obtaining lamellae with thicknesses of 100 μm. Afterward, the material was submitted to a thermal recrystallization treatment of 1,100°C for 1 h in a quartz furnace with the purpose that the irradiated sample would remain defect-free (dislocations, precipitates, etc.). The chilling process was carried out by means of a stream of compressed air. Finally, it was mirror-polished mechanically to attempt to eliminate the major roughness present on the surface.

2.2. Irradiation

For the DIN 1.4970 austenitic-steel samples, we performed, in a Tandentron linear tandem particle accelerator using Ni ions with an energy of 3.66 Megaelectron Volts (MeV), a dose of 360 dpa, and a temperature of 650°C.

The selection of 650°C as the irradiation temperature in this study is based on several technical and operative crite-

ria that reflect the thermal conditions and the mechanisms of behavior of the austenitic stainless steels in advanced nuclear environments. The next-generation reactors, such as the High-Temperature Gas-Cooled Reactors (HTGR) and the International Thermonuclear Experimental Reactors (ITER)-type nuclear fusion reactors, operate at temperatures much higher than the traditional reactors, with fluid coolants that can exceed 500°C and reach up to 700°C. A temperature of 650°C is critical for the design of structural materials such as DIN 1.4970 austenitic stainless steel, which should maintain its structural integrity and resistance to corrosion under irradiation. This temperature simulates realistic conditions that the material could undergo, permitting the study of the distribution and impact of the irradiation-induced defects without destabilizing the austenitic phase.

In addition, at 650°C, the defects generated by the irradiation accumulate at a greater density and atomic mobility is more active, facilitating the observation of atomic-migration phenomena. This temperature is commonly utilized in prior studies on materials for advanced nuclear reactors, providing a solid base for the results obtained.

2.3. Grazing incidence X-Ray diffraction

Although X-Ray Diffraction (XRD) is an excellent technique for the characterization of crystallization phases, the X-rays can penetrate to a depth of hundreds of micras; thus, Grazing X-Ray Diffraction (GXRD) is a technique in which the beam of the X-rays impinges upon the surface of the sample, therefore, on varying the angle of incidence, information can be obtained about the sample with respect to the depth. With this information, we can analyze the damage caused by the irradiation in function of the depth.

In this work, we employed a Bruker model D8 Discover Diffractometer, using the (GXRD) configuration, which possesses parallel parallel-beam geometry and a Göbel mirror. We employed copper radiation K_1(1.5406).

2.4. X-ray photoelectron spectroscopy

X-Ray Photoelectron Spectroscopy (XPS) consists of employing photons to ionize surface atoms by means of the Compton effect, and of the energy of the expelled electron, which is detected and measured [32]. The energy of the expelled electron is given by:

$$E = h\nu - E_b - \phi, \tag{1}$$

where ν is the frequency of the incident photon, E_b is the energy of the link of the electron, and ϕ the task function of the spectrometer.

This technique turns out to be useful for a surface analysis or it may even be performed by means of ionic decapitation and an analysis of the composition of the material with the depth. In this work, we employed a Thermo Scientific model K-Alpha Spectrometer equipped with a monochromatic X-ray source. Also, we utilized K radiation of Al with an energy of 1486.6 eV, and we carried out an ionic decapitation every 25 nm until reaching a depth of 352 nm, in order to obtain the concentration profiles of the elements Fe, Ni, Cr, and Si in terms of the depth.

2.5. Transmission electron microscopy

For observation by Transmission Electron Microscopy (TEM) of the DIN 1.4970 steel, we carried out a preparation of the sample in transversal section with the aid of the double-beam Multi-indicator Multi-indicator-assisted Dynamic Bees Algorithm (MIDBA) (FIB) technique, due to that the employment of the TEM technique requires that the samples be transparent to the electrons; generally, the thickness of the sample should be less than 200 nm. The preparation of samples for their observation by TEM en- tails one of the main problems confronted for analyzing irradiated samples, but even more so if transversal-section preparation is required, the latter essentially needing very long periods of time [31]. At present, these difficulties of preparation in transversal section have been overcome by employing the Ion Beam Focus (IBF) technique.

3. Results, analysis, and discussion

3.1. Results obtained by grazing X-Ray diffraction

We obtained diffractograms of the DIN 1.4970 steel for different angles of incidence, with the purpose of conducting an analysis with the depth. Figure 1 presents the diffractograms of the steel for the Non-Irradiated Zone (NIZ) and for the Irradiated Zone Irradiated Zone (IZ), at distinct angles of incidence: 0.2°, 0.4°, 0.6°, 0.8°, 1°y 2°. The peaks (111) and (200) present in the diffractograms correspond to the austenite phase. On comparing the NIZ with the IZ at different angles of incidence, we can observe that for angles of 0.2° and 0.4°, these corresponding to the NIZ, there is an absence of peaks, while in the diffractograms corresponding to the IZ, the presence is found of the (111) peak, but not the peak of (200), which are characteristic of austenite. The absence of peaks in the NIZ is attributed to the influence of the roughness present on the surface of the steel [see Fig. 2a)].

The roughness present in the sample of the austenitic steel diminishes when the steel is irradiated with ions, the reason for which appreciating the peak (111) is achieved (in the diffractogram corresponding to the IZ). This is confirmed by images obtained with Scanning Electronic Microscopy (SEM) [38], where one may observe an incipient increase of amorphous granules, the morphology typical of oxides in non-irradiated steel, and after the irradiation of these granules, they disappear (Fig. 2).

In addition, in the NIZ of our steel, there is a greater presence of roughness on the surface, which diminishes as the angle of incidence? increases. This change is more notorious in the IZ, in that the peaks corresponding to the austenite phase are found much more defined in this zone. Therefore, we can

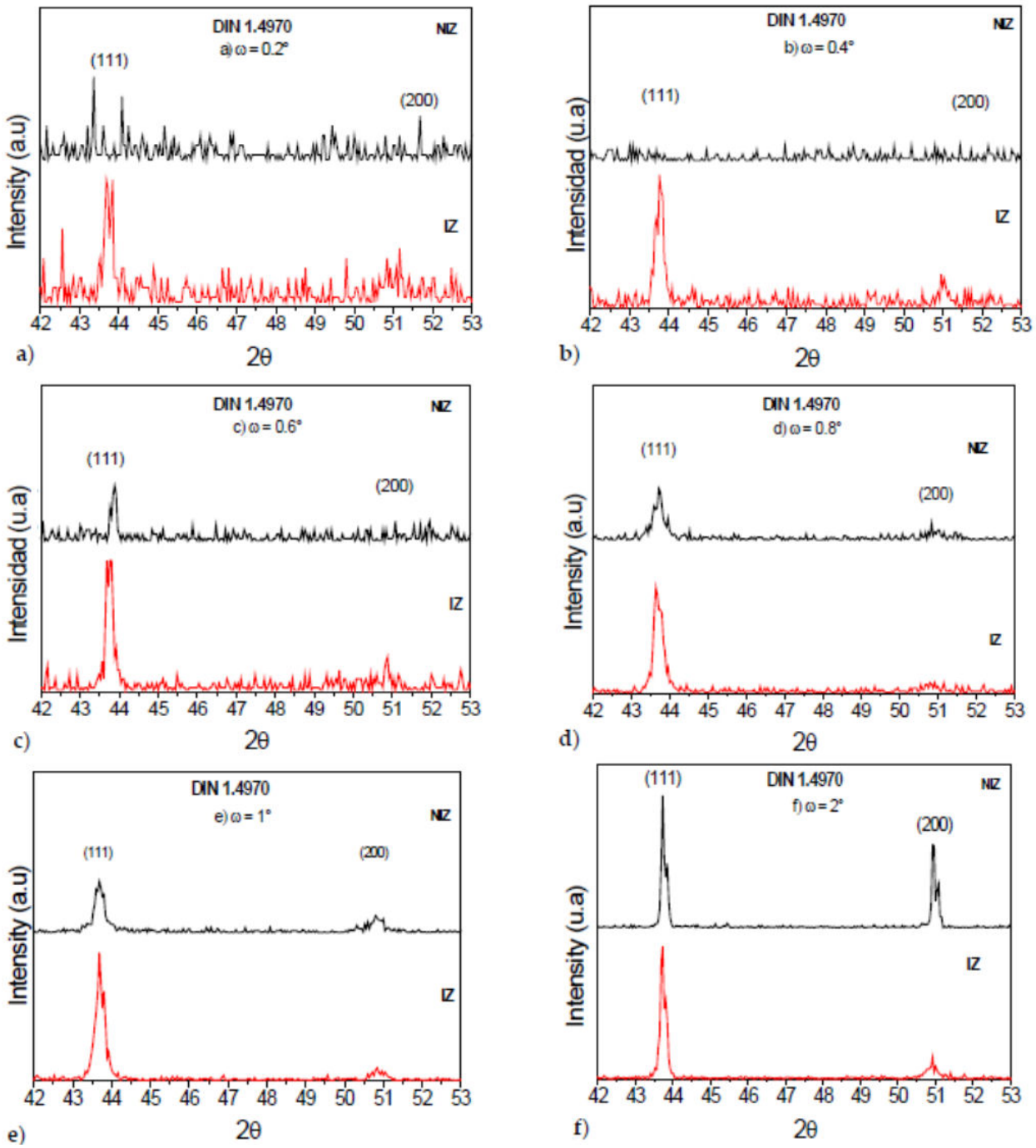

FIGURE 1. X-ray diffractograms of DIN 1.4970 austenitic stainless steel for different incidence angles ω a) ω=0.2°, b) ω=0.4°, c) ω=0.6°, d) ω=0.8°, e) ω=1° and f) ω=2°. The diffractograms in black color correspond to the NIZ while the diffractograms in red color correspond to the IZ.

affirm that, due to the irradiation, the roughness present in this steel diminishes.

It is interesting to note that in the diffractograms of DIN 1.4970 steel, two peaks (111) achieved being resolved around the reflection (111) of the matrix; this double peak can be explained by the variations of the network parameter due to the irradiation [36].

3.2. Results obtained by scanning electron microscopy

In Fig. 2 are shown images obtained by Scanning Electron Microscopy (SEM), in which we can appreciate some monticules with rounded morphologies and brilliant contrast. These monticules appear after the thermal treatment of recrystallization; thus, it is possible that these are precipitates that are generated thermally. Because of their influence on

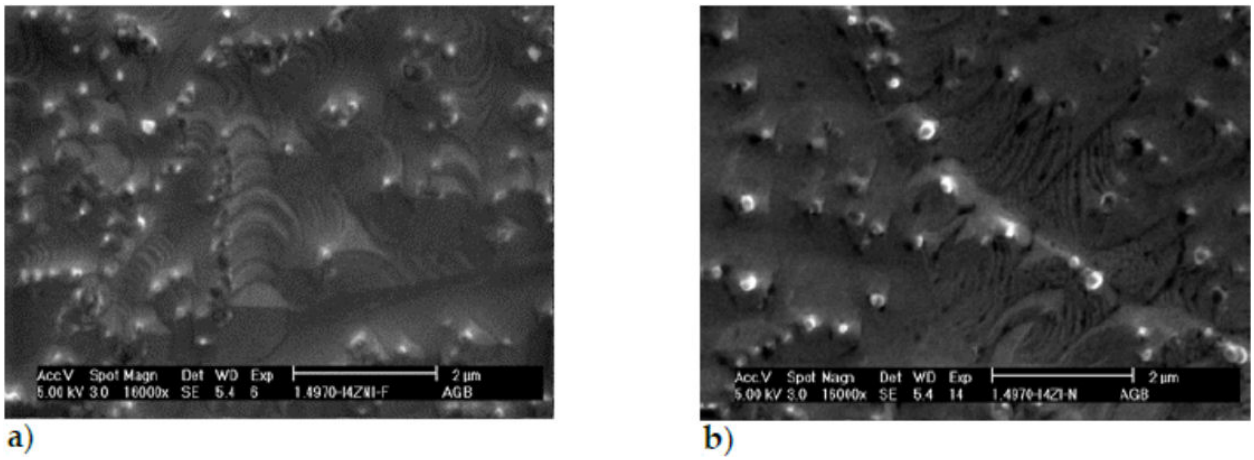

FIGURE 2. Surface morphology by SEM of austenitic stainless steel DIN 1.4970. a) After recrystallization treatment and b) after irradiation with Nickel ions at 360 dpa.

the measurements of roughness, it is necessary to perform a quantification of their density and sizes after each treatment. A first observation is the diminution of the number of monticules after the sample has been irradiated, in that it was found that after the recrystallization treatment, there were approximately 72 monticules per m^2, and that after the irradiation of the steel, the number of monticules diminished to 42 monticules per m^2 [38].

3.3. Results obtained by photoelectron spectroscopy

In Fig. 3 are shown the concentration profiles with the depth of the DIN 1.4970 steel for the NIZ and the IZ. On comparing the concentration profiles between the NIZ and the IZ for the elements Fe, Ni, Cr, and Si, it was observed that the concentration of Fe and Cr in the NIZ is greater with respect to that of the IZ, while the concentration of the elements Ni and Si in the NIZ is lesser with respect to that of the IZ. Thus, we are able to state that, due to the irradiation, there was a decrement of Fe and Cr and an increment of Ni and Si. On the other hand, on conducting the analysis of the concentration of the elements with the depth, we observed the following: for the NIZ, there is a decrement of Fe on the surface, that is, the Fe increases as the depth does. For the case of Si, the behavior exhibited is contrariwise, in that the concentration of this element is greater on the surface and diminishes as the depth does. With respect to the Ni and Cr, there is no variation with the depth. Once the steel was irradiated with Ni ions, changes were also observed in the concentration of these elements in terms of the depth. There is a diminution of Fe and Cr on the surface and an increases of Ni and Si. As the depth of the analysis increases, the concentration of Fe and Cr increases, but the NI and Si decrease their concentration in terms of the depth. The behavior of Si and Cr is in agreement with the mechanisms of migration of the elements under irradiation; however, Ni behaves in a man- ner contrary to that of these mechanisms; this is explained as due to the high doses of irradiation (360 dpa), where it has been reported that for high doses, there is an investment in irradiation-induced segregation [13]. Segregation is the accumulation or enrichment of an element in a localized zone of the material and the subsequent impoverishment of the same in another zone. At elevated temperatures, irradiation with energetic particles induces the spatial distribution of the solutes and solvent of an alloy. This phenomenon leads to an enrichment or impoverishment of the elements of the alloy in regions in close proximity to the surface, dislocations, and grain boundaries.

Under normal conditions, the alloying elements of austenitic stainless steel tend to distribute themselves homogeneously or to segregate themselves according to the temperature and the forces of attraction-repulsion among atoms. However, under irradiation, the crystalline structure undergoes a continuous flow of atomic displacements due to the cascade of collisions caused by high-energy neutrons. This introduces a non-thermal atomic transport, known as radiation-enhanced diffusion.

The inversion in segregation in DIN 1.4970 austenitic stainless steel at high irradiation doses is due to various factors related with atomic mobility and the formation of defects. At high doses of irradiation, the energy supplied causes the atoms in the structure of the steel to be displaced more easily. This can lead to a redistribution of the alloying elements, such as Nickel (NI), Chromium (Cr), and Molybdenum (Mo), which tend to move toward areas of less energy, such as the grain boundaries [39]; additionally, irradiation generates a great amount of vacancies (empty spaces where the atoms should be) and dislocations (defects in the crystalline structure). These defects serve as sites of attraction for certain elements, changing their original distribution and causing inversion in segregation. In Titanium (Ti)-stabilized austenitic steels, such as DIN 1.4970, irradiation can induce the formation of secondary-phase precipitates. These precipitates can interact with the alloying elements, altering their distribution and contributing to inversion in segregation [40]. At elevated temperatures, atomic mobility is even greater, which facilitates the migration of atoms and the formation of defects. This intensifies the effects of the irradiation and

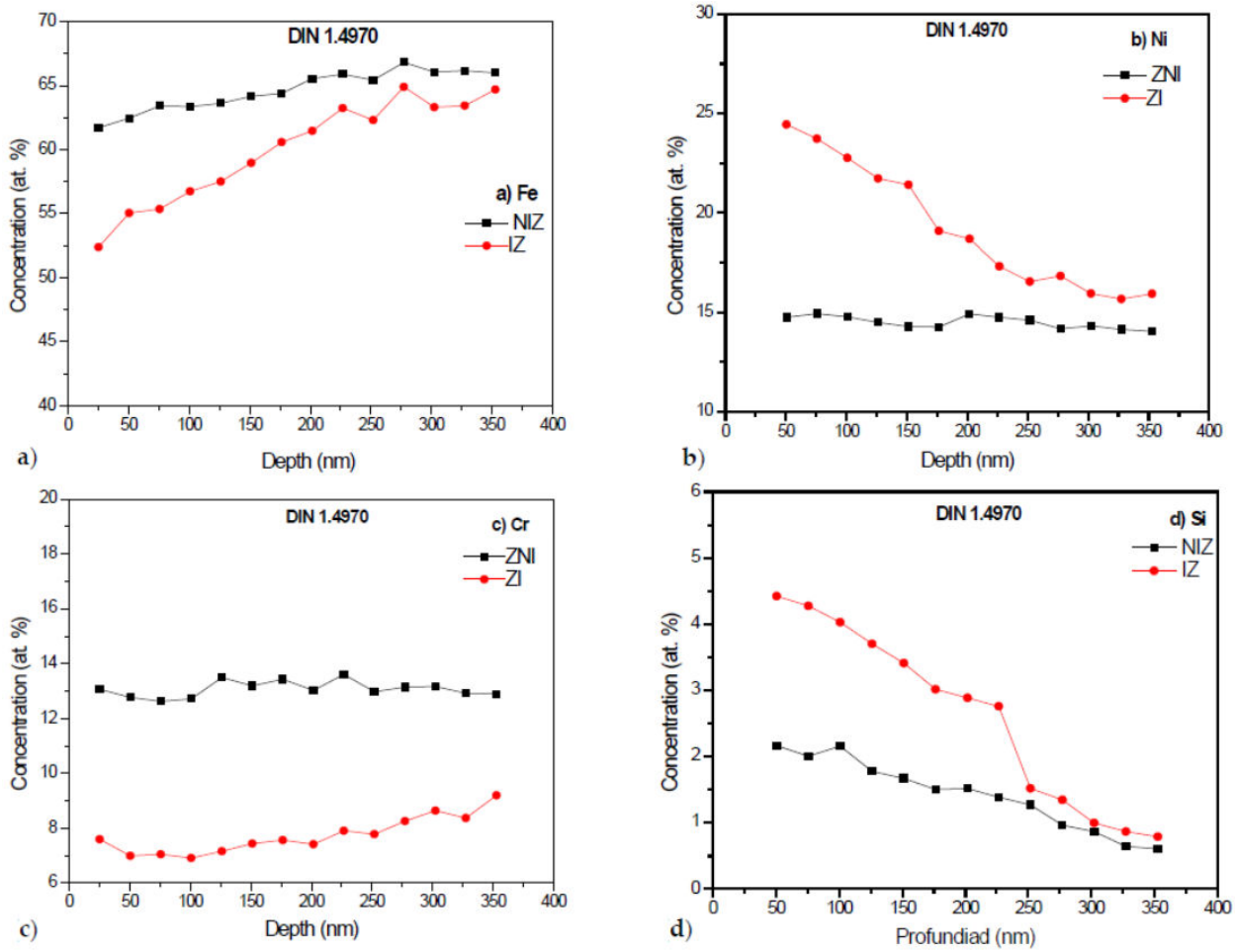

FIGURE 3. Concentration profiles with the depth of austenitic stainless steel DIN 1.4970 in the NIZ (black color) and the IZ (red color), for a) Iron, Fe; b) Nickel, Ni; c) Chromium, Cr and d) Silicon, Si.

promotes the inversion of segregation. In summary, the combination of high-energy irradiation, the formation of defects, and the high temperature give rise to a redistribution of the alloying elements of DIN 1.4970 austenitic stainless steel, resulting in the inversion of segregation.

3.4. Results by transmission electronic microscopy

For observation by Transmission Electronic Microscopy (TEM), we carried out a preparation of the sample in transversal section with the aid of the FIB technique. Figure 4 presents a panoramic image that depicts this transversal section, in which the IZ and the NIZ can be observed. The contrast can be observed in these two zones, the darkest region corresponding to the IZ. In addition, it was observed that the maximal depth of damage caused by the Ni ions is found below the surface.

In Fig. 5 there is presented a sequence of images that includes those from the sample surface that encompasses the IZ up to the zone behind the damage. In these images, we may observe the damage generated by the irradiation of Ni ions with the depth. A variation in contrast is observed that we can associate with the density of the dislocations present

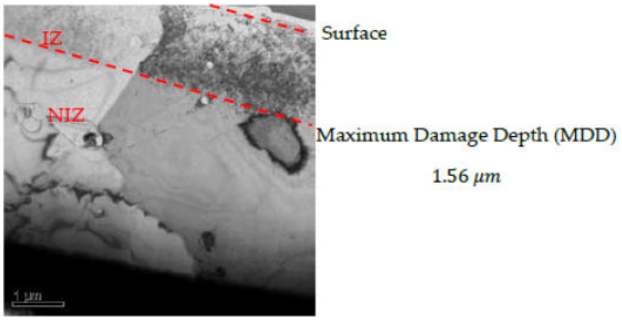

FIGURE 4.TEM image of the cross section of DIN 1.4970 austenitic stainless steel. The NIZ and the IZ are observed.

in the damaged zone, in such a way that a greater concentration of defects in present in the zone of maximal damage found at 1.2 m.

The Maximum Depth-Damage (MDD) whose values correspond to 1.2 μm and 1.56 μm were obtained with two different techniques and derived from complementary focuses. The value of 1.2 μm was obtained through stimulation with SRIM software, which calculates the penetration of Ni ions and the maximal range of ions in the material. This value re-

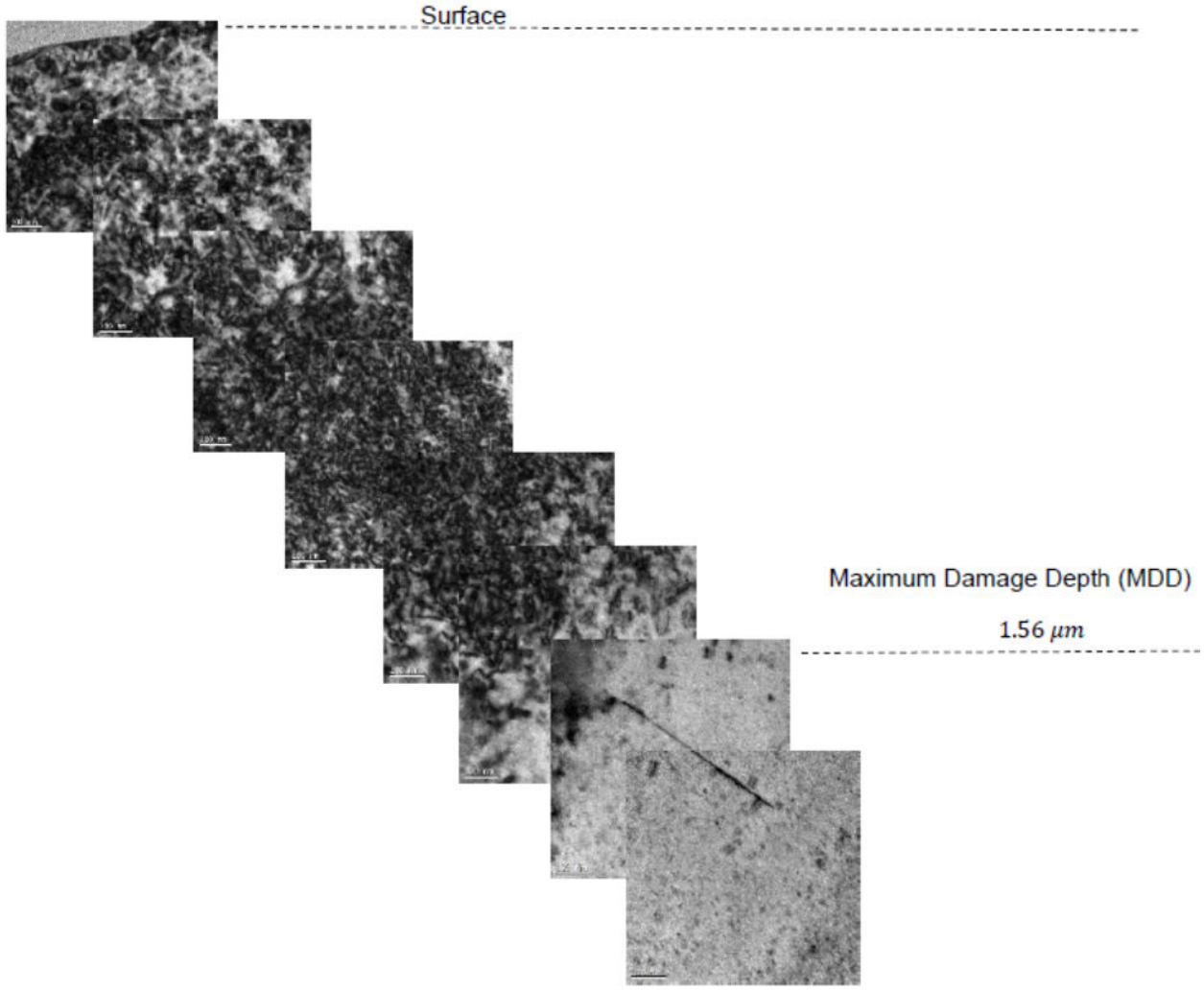

FIGURE 5. Sequence with the depth of damage due to irradiation of DIN 1.4970 austenitic stainless steel.

flects the maximal distance covered by the ions prior to their losing energy; conversely, the value of 1.56 micras derives from direct measurement by means of Transmission Electron Microscopy (TEM), which shows the depth of the damage observed through irradiation-induced dislocation images. The difference between both values is due to that SRIM simulation does not consider the precise defect distribution, while that of TEM provides a more detailed representation of the microstructure and the accumulation of defects. Thus, the experimental measurement reflects the real damage depth with greater precision. Both methods complement the understanding of the damage induced by irradiation, but in a complementary fashion they offer valuable perspectives from different focuses. While SRIM simulation [41] provides a theoretical view of the ions' range of penetration, the TEM technique allows for a direct and detailed evaluation of the structural damage, revealing the accumulation of defects at the microscopic level. The difference between the values obtained highlight the limitations of each technique, but on combining both of these latter, a more complete and precise panorama of the behavior of DIN 1.4970 austenitic stainless steel is obtained.

4. Conclusions

In this study on the implantation of energetic particles, the true depth of the damage induced by the material depends on a series of factors that include the range of penetration of the ions, the density of defects generated, and the measurement method employed. The range of ions, that is, the penetration of the latter into the material, is determined by the energy and the mass of the energetic particles. In the case of the irradiated particles, such as the Ni ions in this study, the interaction between the ion and the material generates depth-dependent damage. As the ions lose energy, their capacity to interact with the material diminishes, implying that the damage is distributed throughout the entire depth.

By means of Grazing Incidence X-Ray Diffraction (GIXRD), we found a diminution in the intensity of the diffraction peaks in the NIZ and the IZ due to the presence

of roughness on the surface. This roughness diminishes once the DIN 1.4970 steel has been irradiated, as observed in the images obtained by means of SEM. Variation in peak intensity (111) at different angles of incidence can be associated with the inhomogeneity in terms of the depth of the concentration of crystalline defects. The results obtained by XPS demonstrate a diminution of Fe and Cr on the surface and an increase of Ni and Si once the DIN 1.4970 steel was irradiated. As the depth of the analysis increases, the concentration of Fe and Cr increases but the Ni and Si diminish in concentration in terms of the depth. The behavior of the Si and Cr are in agreement with the mechanisms of migration under irradiation; however, the Ni behaves in a manner contrary to these mechanisms, this latter explained as due to the high doses of irradiation (360 dpa). On comparing the profiles of concentration between the NIZ and the IZ for the elements Fe, Ni, Cr, and Si, it is observed that the concentration of Fe and Cr in the NIZ is greater with respect to the IZ, while the concentration of the elements Ni and Si in the NIZ is lesser with respect to the IZ. Therefore, we can say that, due to the irradiation, there was a decrease of Fe and Cr and an increase of Ni and Si. Finally, by TEM it was observed that the damage caused by the NI ions inflicted on the DIN 1.4970 steel is found 1.560m below the surface.

On conducting irradiation assays in research reactors, such as the Jules Horowitz Reactor (JHR) in France https://www.revistanuclear.es/wp-content/uploads/hemeroteca/308/NE308-04.pdf, these assays would permit the evaluation of the behavior of DIN 1.4970 austenitic stainless steel under conditions of irradiation similar to those of an operative nuclear reactor. Mechanical and microstructural properties can be measured before and after irradiation to identify changes and to validate the laboratory results. Also, thermohydraulic and neutronic simulations can be developed to replicate the conditions of operation of a nuclear reactor. These simulations can aid in predicting how DIN 1.4970 austenitic stainless steel will behave under different scenarios of irradiation and temperature, providing valuable data for the extrapolation of results.

Acknowledgements

Secretaría de Investigación y Posgrado, Instituto Politécnico Nacional y CONAHCYT.

1. M. Griffiths, Effect of neutron irradiation on the mechanical properties, swelling and creep of austenitic stainless steels, *Materials* **14** (2021) 2622, https://doi.org/10.3390/ma14102622.
2. P. J. Maziasz and J. T. Busby, Properties of austenitic steels for nuclear reactor applications (Elsevier Ltd., Ox ford,UK, 2020), p. 303.
3. B. Radiguet *et al*., Irradiation behavior of nanostructured 316 austenitic stainless steel, *J. Mater. Sci.* **43** (2008) 7338, https://doi.org/10.1007/s10853-008-2875-8
4. W. Daenner, A comparison of AISI type 316 and German type DIN 1.4970 stainless steel with regard to the first-wall lifetime, *J. Nucl. Mater.* **103** (1981) 121.
5. W. Kesternich, Dislocation-Controlled precipitation of TiC particles and their resistance to coarsening, *Philos. Mag.* **52** (1985) 533, https://doi.org/10.1080/01418618508237645
6. K. Ehrlich, Irradiation creep and interrelation with swelling in austenitic stainless steels, *J. Nucl. Mater.* **100** (1981) 149, https://doi.org/10.1016/0022-3115(81)90531-6.
7. F. A. Garner, Radiation-Induced Damage in Austenitic Structural Steels Used in Nuclear Reactors In Comprehensive Nuclear Materials, Second Edition. (2020) 157-158, https://doi.org/10.1016/B978-0-12-803581-8.12067-3.
8. S. Kasahara *et al*., Effect of Mn addition on decrease of Cr depletion at grain boundary in austenitic alloys irradiated with electrons, *J. Nucl. Mater*. **239** (1996) 194, https://doi.org/10.1016/S0022-3115(96)00468-0.
9. N. Cautaerts *et al*., Thermal creep properties of Ti-stabilized DIN 1.4970 (15-15Ti) austenitic stainless steel pressurized cladding tubes, *J. Nucl. Mater.* **493** (2017) 154, https://doi.org/10.1016/j.jnucmat.2017.06.013.
10. L. H. Wang *et al*., Effect of prior thermal treatment on the microchemistry and crack propagation of proton-irradiated AISI 304 stainless steels, *J. Nucl. Mater*. **328** (2004) 11, https://doi.org/10.1016/j.jnucmat.2004.02.003.
11. M. Terada *et al*., Microstructure and intergranular corrosion of the austenitic stainless steel 1.4970, *J. Nucl. Mater*. **358** (2006) 40, https://doi.org/10.1016/j.jnucmat.2006.06.010.
12. N. Cautaerts *et al*., The role of Ti and TiC nanoprecipitates in radiation resistant austenitic steel: A nanoscale study, *Acta Mater*. **197** (2020), https://doi.org/10.1016/j.actamat.2020.07.022.
13. W. Kesternich and A. Garcia-Borquez, Inversion of the radiation-induced segregation behaviour at grain boundaries in austenitic steel, *Scripta Mater*. **36** (1997) 1127, https://doi.org/10.1016/S1359-6462(97)00004-3.
14. N. Cautaerts *et al*., Characterization of (Ti,Mo,Cr) C nanoprecipitates in an austenitic stainless steel on the atomic scale, *Acta. Mater.* **164** (2019) 90, https://doi.org/10.1016/j.actamat.2018.10.018.
15. J. Titchmarsh and S. Dumbill, On the measurement of radiation-induced segregation (RIS) at point defect sinks, *J. Nucl. Mater.* **227** (1996) 203, https://doi.org/10.1016/0022-3115(95)00159-X.

16. F. Onimus *et al*., *Irradiation Creep in Materials,* **1** (2021), https://doi.org/10.1016/B978-0-12-803581-8.11645-5.

17. P. Yvon, Structural Materials for Generation IV Nuclear Reactors (2016).

18. Y. Yamamoto *et al*., Alumina-Forming Austenitic Stainless Steels Strengthened by Laves Phase and MC Carbide Precipitates, *Metall. Mater. Trans. A* **38** (2007) 2737, https://doi.org/10.1007/s11661-007-9319-y.

19. P. J. Maziasz and C. J. McHargue, Microstructural evolution in annealed austenitic steels during neutron irradiation, *Mater. Sci. Technol.* **32** (1987) 190, https://doi.org/10.1179/095066087790150.

20. D. Koury *et al*., Analysis of bi-layer oxide on austenitic stainless steel, 316L, exposed to Lead-Bismuth Eutectic (LBE) by X-ray Photoelectron Spectroscopy (XPS), *J. Nucl. Mater*. **440** (2013) 28, https://doi.org/10.1016/j.jnucmat.2013.03.093.

21. P. Hosemann *et al*., Characterization of oxide layers grown on D9 austenitic stainless steel in lead bismuth eutectic, *J. Nucl. Mater* **375** (2008) 323, https://doi.org/10.1016/j.jnucmat.2007.12.005.

22. R. V. Nandedkar and W. Kesternich, Effect of boron on high-temperature creep behavior of austenitic stainless steel DIN 1.4970, *Metall. Trans. A* **21** (1990) 3033, https://doi.org/10.1007/BF02647301.

23. E. Longo *et al*., In situ Transmission Electron Microscopy observation of Ag nanocrystal evolution by surfactant free electron-driven synthesis, *Sci. Rep.* **6** (2016) 21498, https://doi.org/10.1038/srep21498.

24. A. Courcelle *et al*., Evolution under Irradiation of Optimized Austenitic Steel For Gen-IV Reactors. Impact on Fuel Cladding Properties and Performances, *EPJ Web Conf.* **115** (2016) 47, https://doi.org/10.1051/epjconf/201611504003.

25. F. A. Garner, Radiation Damage in Austenitic Steels, In R. J. M. Konings, ed., *Compr. Nucl. Mater.* (2012) pp. 33-95.

26. N. Hashimoto *et al*., Microstructure of austenitic stainless steels irradiated at 400° in the ORR and the HFIR spectral tailoring experiment, *J. Nucl. Mater.* **280** (2000) 186, https://doi.org/10.1016/S0022-3115(00)00046-5.

27. H. Huang *et al*., TEM, XRD and nanoindentation characterization of Xenon ion irradiation damage in austenitic stainless steels, *J. Nucl. Mater*. **454** (2014) 168, https://doi.org/10.1016/j.jnucmat.2014.07.033.

28. R. L. Plaut *et al*., Microstructure after Solution Annealing of the Nuclear Grade Austenitic Stainless Steel DIN 1.4970, *Mater. Sci. Forum* **1016** (2021) 1147, https://doi.org/10.4028/www.scientific.net/MSF.1016.1147.

29. E. Charalampopoulou *et al*., Transmission electron microscopy study of complex oxide scales on DIN 1.4970 steel exposed to liquid Pb-Bi eutectic, *Corros. Sci*. **147** (2019) 22, https://doi.org/10.1016/j.corsci.2018.10.018.

30. D. Chen *et al*., The effects of loop size on the unfaulting of Frank loops in heavy ion irradiation, *J. Nucl. Mater.* **529** (2020) 151942, https://doi.org/10.1016/j.jnucmat.2019.151942.

31. A. Garcia-Borquez and W. Kesternich, Controlled-Depth and cross-section preparation techniques for transmission electron microscopy subsurface studies in metals, *Microsc. Res. Tech.* **25** (1993) 255, https://doi.org/10.1002/jemt.1070250307.

32. P. Flewitt and R. Wild, Physical Methods for Materials Characterisation, Graduate student series in materials science and engineering (Inst. Phys. Pub., 1994).

33. H. Schroeder and Y. Dai, Helium concentration dependence of embrittlement effects in DIN 1.4970, 13% cw austenitic stainless steel at 873 K, *J. Nucl. Mater*. **191-194** (1992) 781, https://doi.org/10.1016/0022-3115(92)90578-9.

34. S. Rugel et al., Grazing-incidence X-ray diffraction on ionimplanted silicon, *Appl. Surf. Sci.* **54** (1992), https://doi.org/10.1016/0169-4332(92)90096-G.

35. J. Dudognon et al., Simulation of X-ray diffractograms obtained by grazing incidence X-ray diffraction of implanted stainless steel, *Surf. Interface Anal*. **40** (2008) 441, https://doi.org/10.1002/sia.2638.

36. J. Dudognon et al., Modelling of grazing incidence X-ray diffraction spectra from Mo-implanted stainless steel, *Surf. Coat. Technol.* **200** (2006) 5058, https://doi.org/10.1016/j.surfcoat.2005.05.025.

37. Y. Dai et al., The Effects of Helium in Irradiated Structural Alloys, **1** (2020) 186-234,

38. R. García, Surface modification study in stainlees steel irradiated with 3.66 MeV Ni ions, 1st ed. (Proceeding of XXIX Annual Meeting International Conference on Surface Materials and Vacuum, S.L.P., México, 2009) p. 199

39. N. Flores-Fuentes, Estudio Comparativo por diferentes técnicas, de los cambios microestructurales en aceros austeníticos, inducidos por la irradiación con iones de Ni, Ph.D. tesis, Escuela Superior de Física y Matemáticas, Instituto Politécnico Nacional, México (2013).

40. J. A. Abasolo *et al*., Transmission electron microscopy characterization of radia-tion-induced precipitates with high energy ions in stabilized austenitic steels, Rev. Latim Am. Met **22** (2022).

41. J. Ziegler, SRIM-The Stopping and Range of Ions in Matter, version 2010, In SRIM Software, available at: http://www.srim.org/ (2010).